American Journal of Nanomaterials, 2023, Vol. 11, No. 1, 1-9
Available online at http://pubs.sciepub.com/ajn/11/1/1
Published by Science and Education Publishing
DOI:10.12691/ajn-11-1-1

Gold Nanoparticles Microwave-assisted Synthesis Employing Exclusively Ascorbic Acid as a Reducing and Stabilizing Agent: An Experimental and Computational Study

Ricardo Baez-Cruz[1,2,*], Erik Beristain-Montiel[3,*]

[1]Department of Physics, Faculty of Physical and Mathematical Science, University of Concepcion, PO-Box 160-C, Concepcion, Chile
[2]Max Planck Institute for Polymer Research, Ackermannweg 10, 55128 Mainz, Germany
[3]Facultad de Quimica, Universidad Nacional Autonoma de Mexico, Coyoacan 04510, CDMX, Mexico
*Corresponding author: rbaez@udec.cl, erickbm@comunidad.unam.mx

Received December 10, 2022; Revised January 14, 2023; Accepted January 20, 2023

Abstract Using soft acids as reducing agents in synthesizing metallic nanoparticles have constituted a clear framework for achieving selected morphological properties with minimal toxicity. The system's complexity and the many variables involved represent a challenge for experimental studies desiring to design reproducible synthesis protocols. In this work, we explore the exclusion of any stabilizing agent to synthesize, in an aqueous solution, non-spherical gold nanoparticles (AuNPs) via Microwave-assisted synthesis, and instead, we employed pH control over reducing agent L-Ascorbic acid (AH_2). The use of AH_2 presents a direct approach that allows an understanding of the role of soft acids in synthesizing metallic nanoparticles. The results indicate that AuNPs synthesized at pH $\geq$ 10 exhibit relatively different morphologies than those obtained at higher pH values. The AuNPs were characterized via Transmission electron Microscopy and UV-Vis Spectroscopy. Our simulations reveal the plasmon distribution according to particle shape. The experimental analysis suggests that the pH variation mechanism over the reduction agent correlates with AuNPs geometry. These results indicate that pH is an applicable parameter for controlling the nanoparticle's geometry and extend the possibility of exploring computational studies on the impact of acids adsorbed on gold colloidal surfaces.

Keywords: *gold nanoparticles, wet-synthesis, L-Ascorbic acid, TEM, BEM*

Cite This Article: Ricardo Baez-Cruz, and Erik Beristain-Montiel, "Gold Nanoparticles Microwave-assisted Synthesis Employing Exclusively Ascorbic Acid as a Reducing and Stabilizing Agent: An Experimental and Computational Study." *American Journal of Nanomaterials*, vol. 11, no. 1 (2023): 1-9. doi: 10.12691/ajn-11-1-1.

1. Introduction

Gold nanoparticles (AuNPs) have been widely studied in experimental and theoretical approaches because of their attractive electric and optical properties [1]. Furthermore, the AuNP material is a conductor that, under normal conditions, crystalizes in a face-centered cubic cell (fcc) [2]. Therefore, AuNPs' electric and optical properties can be used in wide-ranging applications [3], such as photovoltaic devices [4], OLEDs [5], perovskite solar cells [6], or photocatalysis [7].

Several methods have been described for synthesizing AuNPs; recently, some authors [8] extended the understanding of the Turkevich method [9], which is considered a milestone in AuNPs preparation. Additionally, a tuning of the AuNP shape was proposed by Murphy. et al. [10] by a seed-mediated growth procedure, and most recent research has tuned particle shape using two different capping agents (surfactants/polymers) [11].

Usually, shape tuning is promoted by using strong reducing and stabilizing agents, such as Ascorbic acid (AH_2) and CTAB, respectively [12]. Numerous applications and synthesis approaches have aimed to control AuNPs' shape since their optical properties, such as the Localized Surface Plasmon Resonance (LSPR) effect [13], strongly depend on the AuNPs' shape [14]. One of the methods used has been micro-wave-assisted synthesis [15]; for example, Kwok Wei Shah et al. achieved hexagonal AuNPs reduced by organosilane [16]. The microwave method avoids side reactions due to selective heating [17,18], in addition to increasing the solution temperature based on direct heating of the sample without using the volumetric flask as an intermediate [19], and offers short synthesis times compared to synthesis routes based on conventional heating [20,21].

Early studies have synthesized spherical AuNPs using ascorbic acid at room temperature, e.g., Himanshu Tyagi et al. obtained a narrow size distribution (31±5, 36±6, and 40±5 nm) of spheroidal AuNPs readily stabilized by adjusting the reaction solutions' initial pH conditions [22].

Later, Shohifah Annur et al. developed spherical AuNPs of different sizes range (20-40 nm) at room temperature by adjusting the pH of ascorbic acid at a range of 2.0 to 10 [23]. However, these methods have obtained only spherical gold nanoparticles, limiting the LSPR effect exclusively to a dipolar field distribution [24]. Moreover, these methods reduced the possibility of getting quadrupolar, hexapolar, and octupolar plasmon field distributions[25]. Therefore, the particle applications range [26] is limited in areas such as bifunctional NO2 light sensing [27], light-sensing devices [28], or photocatalysis process [29,30].

Therefore, the preparation of anisotropic colloidal gold nanoparticles represents an experimental challenge to control the size and morphology to benefit from their excellent optical properties provided by the LSPR effect in various applications.

Consequently, in this work, we have explored an experimental approach to synthesize, to some extent, anisotropic gold colloidal nanoparticles using microwave-assisted synthesis by controlling the pH value of ascorbic acid (AH_2) using it exclusively as both a reducing and stabilizing agent.

2. Materials and Methods

2.1. Reagents and Instruments

All chemicals were of analytical grade and were used without further purification. Gold (III) chloride acid trihydrate ($HAuCl_4{\cdot}3H_2O$) (99.9%) and L-Ascorbic acid($C_6H_8O_6$) (99%) (AH_2) were purchased from Sigma-Aldrich. Sodium hydroxide (NaOH, pastilles, from Molar) was used to adjust the pH. The water used in all experiments was prepared using a Milli-Q Integral water purification system (EMD Millipore Direct -Q® 3UV-R) and had a resistivity of 18.2 MΩ cm. Samples were prepared using a CEM Focused Microwave™ Synthesis System, with a continuous microwave power delivery system with operator-selectable power output from 0- 300 watts. Optical absorption studies were carried out using an ultraviolet-visible–near-infrared (UV-vis-NIR) spectrophotometer (JASCO V-670). Particle size and morphologies were studied using a transmission electron microscope (TEM, JEOL JEM-2010). Interplanar spacing in the AuNPs was studied using high-resolution (HR)-TEM (Tecnai F20 microscope with FEI, acceleration voltage 200kV).

2.2. Sample Preparation

Unifactorial experiments with two replicates optimized synthetic conditions. First, different molar ratios of $HAuCl_4$, AH_2, and pH were tested. Briefly, 50 ml of 100 mM AH_2 solution was prepared and separated into vials of 4.5 ml. Next, different Molar ratios R = [NaOH]/[AH_2] were tested to obtain a pH variation on each sample (R from 0 to 2, steps of 0.2 each). The NaOH/AH_2 mixtures were left in closed vials under constant stirring for three hours at room temperature under ambient conditions to reach pH equilibrium. Then, at room temperature, 45 µl of each pH-adjusted AH_2 solution was added to 4.5 ml of a 0.5 mM fresh Gold (III) chloride acid trihydrate ($HAuCl_4{\cdot}3H_2O$) solution. The mixtures were immediately mixed and radiated at 200°C, 15 bar, and 300 W for 30 sec using a microwave reactor system. The samples were left to cool down at room temperature without an external cooling source. Subsequently, the samples were centrifuged at 1000 rpm, and the supernatant was extracted as the final product.

2.3. Characterization

The ImageJ software, with standard plugins, was implemented to determine particle distribution and population, with a minimum of 56 particles per micrograph. The polydispersity (P) was estimated employing the standard Equation 1:

$$x = \frac{\sigma}{s}100\% \quad (1)$$

Where **σ** is the standard deviation, **σ** = FWHM/2, FWHM is the full width at half maximum of the total distribution, and **s** is the mean particle diameter (in nm) [31]. Gatan Digital-Micrograph software was used to analyze the (HR)-TEM micrographs. In addition, the crystallographic toolbox (CrysTBox) software was used to study diffraction patterns obtained from (HR)-TEM micrograph [32].

2.4. Simulation of Optical Properties

We used the boundary element method (BEM) [33] to calculate the electric field distribution and the local photonic density of states (LDOS) [34] on the gold nanoparticles. We implemented the methodology described in the MNPBEM (Metallic Nano Particles BEM) MATLAB toolbox [35,36]. The underlying idea of the BEM method is to solve Maxwell's equations for a dielectric system. The system is modeled as elements with homogeneous and isotropic dielectric functions separated by sharp interfaces [37,38]. Hence, the method employs a geometrical mesh to discretize the interfaces aiming at solving Maxwell's equations using the proper boundary conditions [39,40,41]. Input parameters were the absorption wavelength, particle size, and particle shape obtained from the experimental results of steady-state absorption studies and TEM measurements. In addition, the optical constant for bulk gold was obtained from reference data [42].

3. Results

3.1. Synthesis of AuNPs

The reduction of gold was achieved by employing only AH_2 in a pH-controlled solution. The proposed method produced AuNPs in red color solutions with increasing intensity concerning pH value (see Figure S2-Supplementary Material). At molar ratios (R) greater than 1.2 (pH ≥ 10), the more intense color was obtained and remained unchanged at higher R. As will be discussed later, this result was directly related to the morphology of AuNPs. In this regard, the AuNPs synthesized at pH = 10 were chosen for further analysis.

3.2. Morphological Characterization

TEM image (Figure 1) shows AuNPs (at 100 nm resolution) obtained by reacting gold (III) ($HAuCl_4 \cdot 3H_2O$) with AH_2 at pH 10. This image shows that the pH reaction conditions yield non-spherical particles with increasingly amorphous shapes. The average particle size was determined by analyzing twenty TEM micrographs and a minimum of 56 particles per micrograph (Supplementary Material Figure S1 shows a gallery of a portion of TEM micrographs used to calculate the particle size distribution pH 10) and standard imaging protocols with the ImageJ software package. The results from the particle size study are given in the histograms in Figure 1(b). A Gaussian fit to the size distribution shows that the pH 10 reaction conditions yield 25 ± 13 nm diameter particles. The polydispersity for the sample set was calculated as 52%.

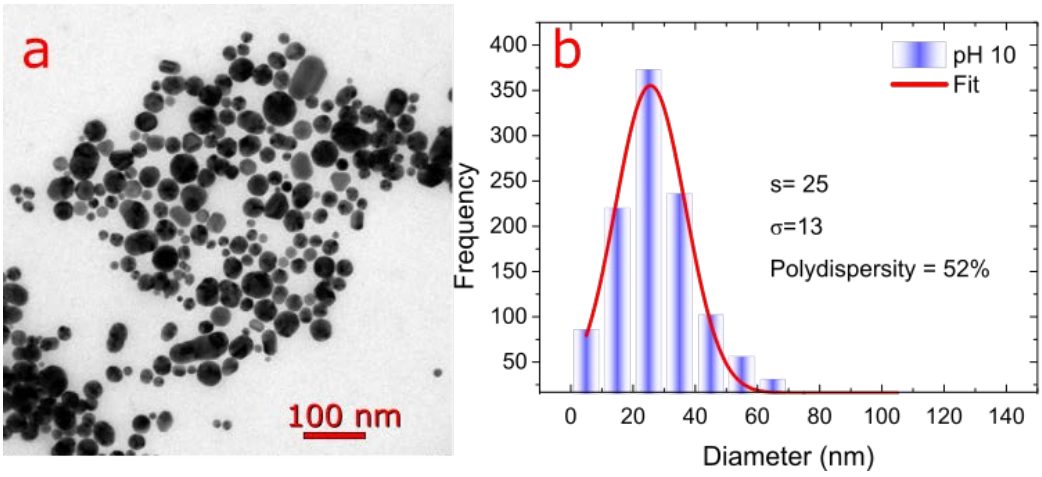

Figure 1. Morphological characterization with electron microscopy shows that different sizes and shape distributions emerge when AuNPs are synthesized with AH_2 at pH 10. (a) Electron microscopy micrograph, with a resolution of 100 nm, shows AuNPs distribution synthesized at pH 10. (b) Histogram of the AuNPs size distribution at pH 10 with a frequency over 400 counts

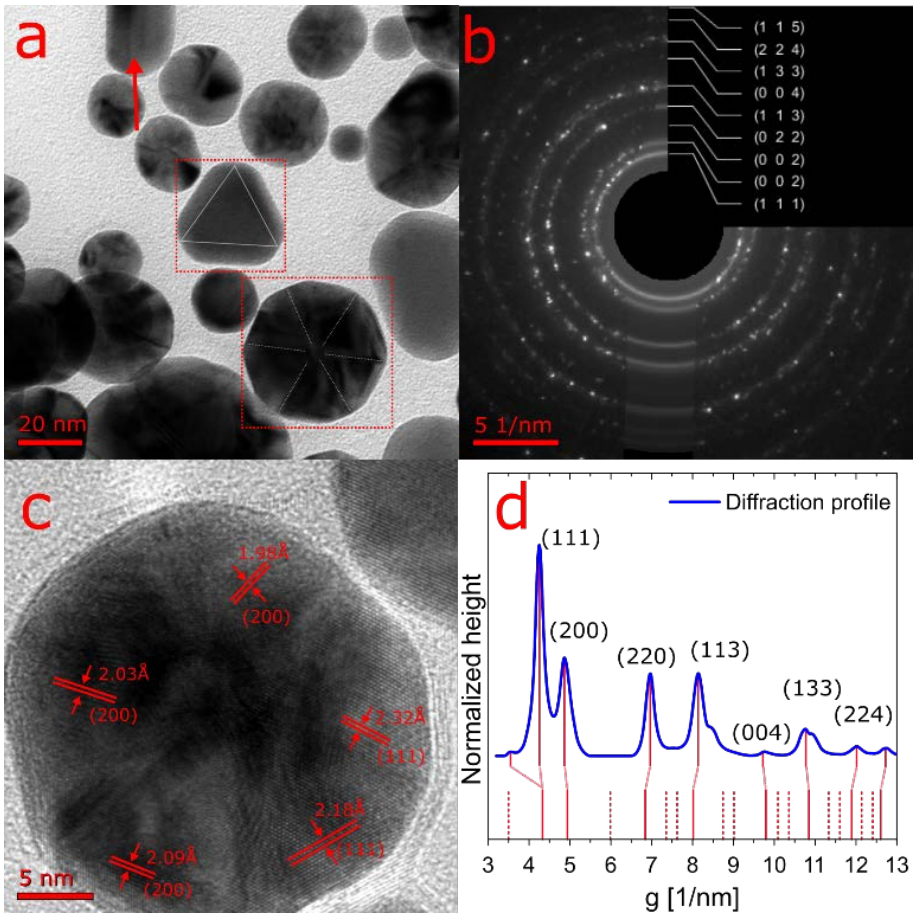

Figure 2. Crystalline structure characterizations of AuNPs with electron microscopy shows different shape emerge at pH 10. (a) Electron microscopy micrograph, with a resolution of 20 nm, shows the different shapes of AuNPs (b) Electron diffraction pattern of AuNPs. (c) High-resolution TEM micrograph at 5 nm of resolution. (d) The electron diffraction profile of image (b) shows the (111), (200), (220), and (311) orientation of gold in a typical fcc structure

Figure 2(a) shows a TEM image of 20 nm resolution, suggesting different particle shapes. The electron diffraction pattern from the TEM measurements is shown in Figure 2(b). The primary diffraction peaks correspond to (111), (200), (220), and (113) reflections, which are characteristic of the gold fcc structure[2]. The surface structure of the particles was further analyzed using high-resolution TEM, as shown in Figure 2(c). Two well-resolved (111) and (200)-type crystallographic planes were detected (measured D-spacing of about 2.32 Å and 2.03 Å, which run perpendicular to the sidewalls of the structure. Figure 2(d) shows the corresponding electron diffraction profile from Figure 2(b) for the nanoparticles set at pH 10. Again, the diffraction peaks' relative intensities vary, suggesting a difference in the particle shape, as Figure 2(a) shows.

3.3. Steady-state Absorption Gold Nanoparticles

The AuNPs' optical absorption spectrum was studied between 400 to 800 nm and was fitted as a sum of Gaussian functions [43]. The synthesized sample exhibit a typical AuNPs absorption peak over ~525 nm (Figure 3(a)), which corresponds to absorbed green light and agrees with Localized Surface Plasmon Resonance (LSPR) frequency ($\boldsymbol{\omega}$) from previous AuNPs reports [44]. Figure 3(b) shows the scattering cross-section ($\boldsymbol{\sigma}_{Sct}$) result computed numerically for a 25 nm diameter AuNP and an incoming plane wave excitation polarized along $\boldsymbol{x}$, between 400 to 800 nm. The 25 nm diameter AuNPs' light scattering was calculated using the MNPBEM toolbox [35,36], and the size obtained in the histogram analysis (Figure 1(b)) was used as the input parameter. As a result, a value of approximately 26 nm^2 was obtained for $\boldsymbol{\sigma}_{Sct}$. Figure 3(a-b) shows that the scattering and absorption spectrum's peaks consist primarily of yellow and green light [45]. Therefore, the non-scattered or absorbed light compounds the red transmitted light by the sample (image color sample Figure 3(a)).

3.4. Simulations Results

A qualitative study of electric field distribution (EFD) and the electron energy loss probability of the synthesized AuNPs were computed using the simulation toolbox MNPBEM for plasmonic nanoparticles [35,36]. First, the EFD has computed considering four radiation conditions described by the combination of indices $\mathbf{u}^i_\alpha$; i with i=1,2,3 indicating the polarization direction (1= x, 2 = y, and 3 = z) [46] and (x, y, z) the direction of the incident field (525 nm obtained from the Absorption spectrum, Figure 3). Then, based on the TEM results (Figure 2(a)), the EFD was calculated for a nanosphere, nanotriangle, and nanohexagon, as shown in Figure 4(a). The results show that although the incident field is the same (525 nm), the EFD around the particles changes as the incident field polarization changes, which is associated with the particle shape influence over the plasmon distribution of metallic nanoparticles[35,36].

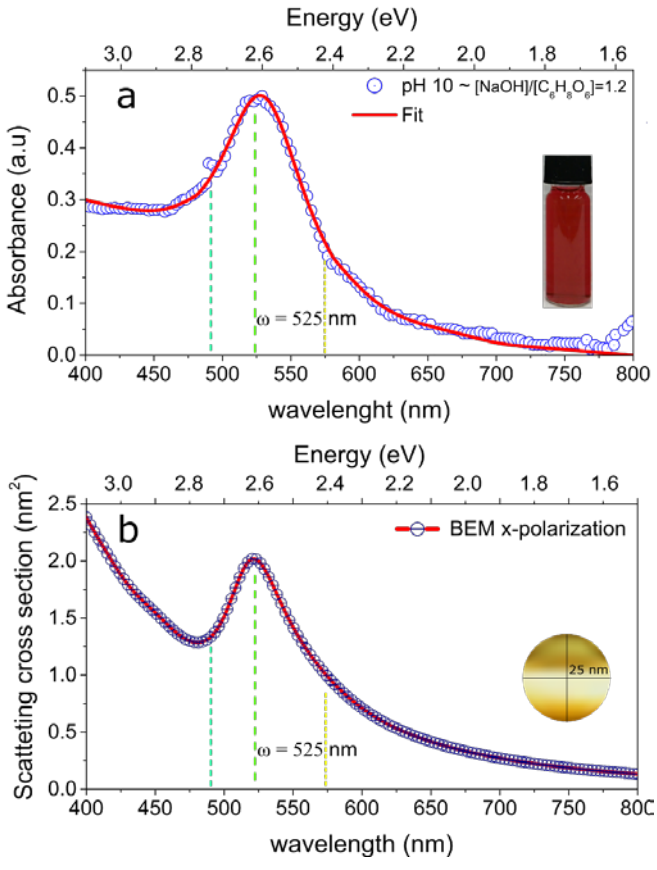

Figure 3. (a) Absorption spectrum of synthesized AuNPs pH 10. The data were curve-fitted using Gaussian functions to identify the principal peak contribution. The spectrum exhibits an absorption peak over ~525 nm. (b) Scattering cross-section ($\boldsymbol{\sigma}_{Sct}$) of a gold nanoparticle of 25nm diameter computed using the MNPBEM toolbox. A scattering peak at around 525 nm was localized. The absorption and Scatter spectra explain the color of the sample

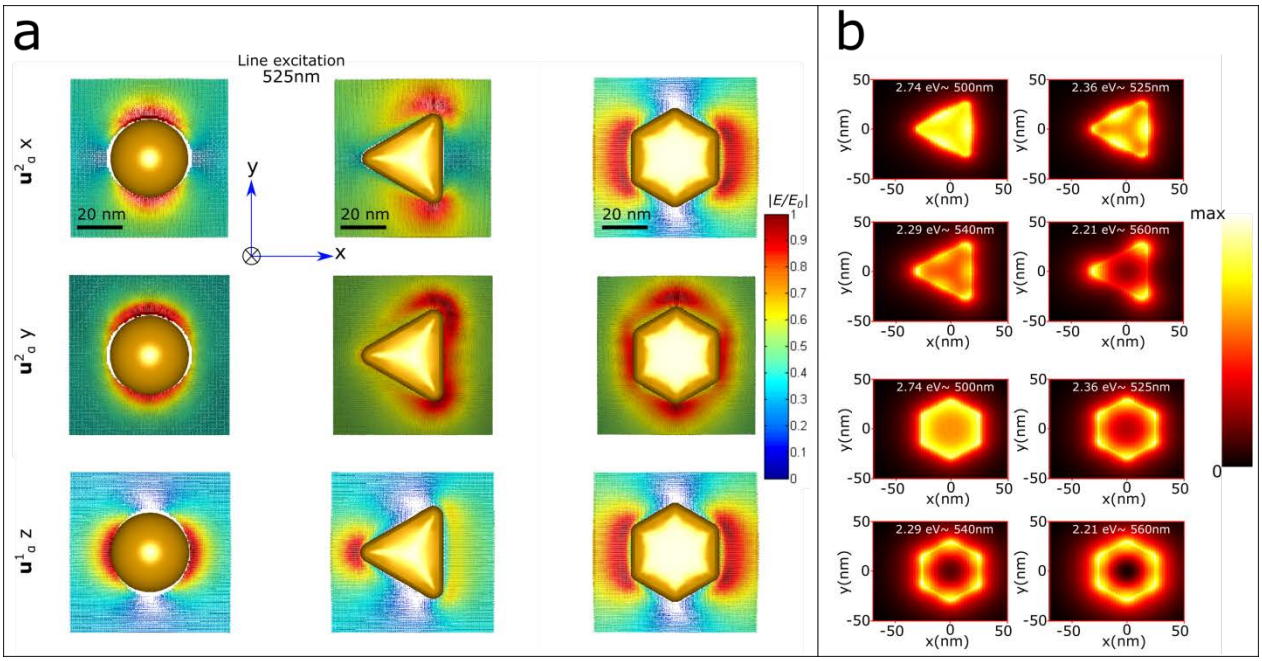

Figure 4. (a) Electric field distribution (EFD) computed using the simulation toolbox MNPBEM in the boundary of AuNPs with an equivalent shape to the synthesized particles. The particles are excited by 525 nm with polarization direction $\mathbf{u}^i_\alpha$: i with i=1,2,3 (1= x, 2 = y, and 3 = z). (b) EELS probability map computed using the simulation toolbox MNPBEM, with an impact excitation energy of 2.74, 2.36, 2.29, and 2.21 eV for both shape particles

However, more precise information on plasmonic states in metallic nanoparticles is required for many applications, such as photonic or optoelectronic devices [47,48,49]. A technique such as Electron energy loss spectroscopy (EELS) is an effective tool for investigating plasmon modes in single and coupled metallic nanoparticles [50,51,52]. Thus, the EELS probability map for the same single nanotriangle and nanohexagon was additionally computed. In a 50nm square grid, the nanoparticles were localized at 10 nm from the plane, as shown in Figure 4(b). The particles were impacted with 2.74, 2.36, 2.29, and 2.21 eV, equivalent to the local wavelength values in the maximum absorption point (Figure 3). The results show that once the particles are excited with photons of 2.74 eV ~500nm, above the resonance energy (2.36 eV~ 525nm), the plasmon distribution for both particles is localized in the particle surface, as shown in Figure 5b - 2.74eV case. When the particles are excited with the resonance energy, 2.36 eV~ 525nm, the plasmon field adopts a different distribution for both particles and is localized on the edge of the particles (Figure 4b - 2.36eV case). A similar distribution is localized for the photoexcitation cases 2.29eV~540nm and 2.21 eV~560nm.

4. Discussion

TEM results (Figure 2) showed that, on average, particles associated with pH 10 were approximately 70% bigger than the particles obtained by different synthesis reaction pH approaches [53]. Earlier works had shown that when AH_2 was used as a reducing agent to produce AuNPs, the size and shape did not depend on the reactant concentrations [54,55]. Previous results showed that pH control over AH_2 induces size particle change [22,23]. However, our tuning-pH approach synthesis demonstrates not only size particle change but also induces particle shape, as shown in the TEM results from Figure 2(a and d) and Figure S2-supplementary material. Earlies microwave-assisted synthesis has obtained self-supported superstructures based on 1-dodecanethiol [56,57], known for its excellent properties as a sulfur source, capping ligand, and size controller [58]. This synthesis approach's success is based on stabilizing agents such as 1-dodecanethiol, poly(vinyl pyrrolidinone) (PVP) [15], or CTAB [59]. In comparison, the results obtained in this investigation show the possibility of conjugating non-spherical gold nanoparticles with the exclusive use of AH_2 as a reducing agent and a microwave source (Figure 2(a and d) and Figure S2-supplementary material).

In general, below pH 10, AuNPs were formed as conglomerated spherical particles. However, at pH ≥ 10, a more discrete size distribution (25 ± 13 nm) was obtained. An explanation of the pH effect on AuNP morphology is shown in Figure 5. This mechanism was based on the results of a recent depth analysis of the oxidation mechanisms of ascorbic acid [60].

Multiple AH_2 molecules can be coordinated to Au^{3+} atoms since AH_2 have multiple positions with high electronic density (hydroxyl groups). As increasing pH, AH_2 is deprotonated to form ascorbate AH-. An electron from each coordinated AH- is transferred to Au^{3+} to reduce it to Au^0, producing a radical AH·. As the pH increased, the second pka was reached, and the second deprotonation of ascorbic acid took place to form the radical anion A.-. This process started occurring at pH ≥ 10. Later, the second release of an electron from each A.- equivalent reduced Au^{3+} to Au^0, and dehydroascorbate A was finally formed. Note that at increasing pH with every deprotonation of ascorbic acid, anionic species were formed, then the negative charge of the corresponding ascorbates was available to coordinate to Au^0 and stabilize the AuNPs. In other words, increasing pH not only improved the reductive effect over gold but also decreased the possibility of multiple coordination positions of ascorbic acid to the Au^0 atoms, stabilizing the structure and forming more regular shapes of AuNPs.

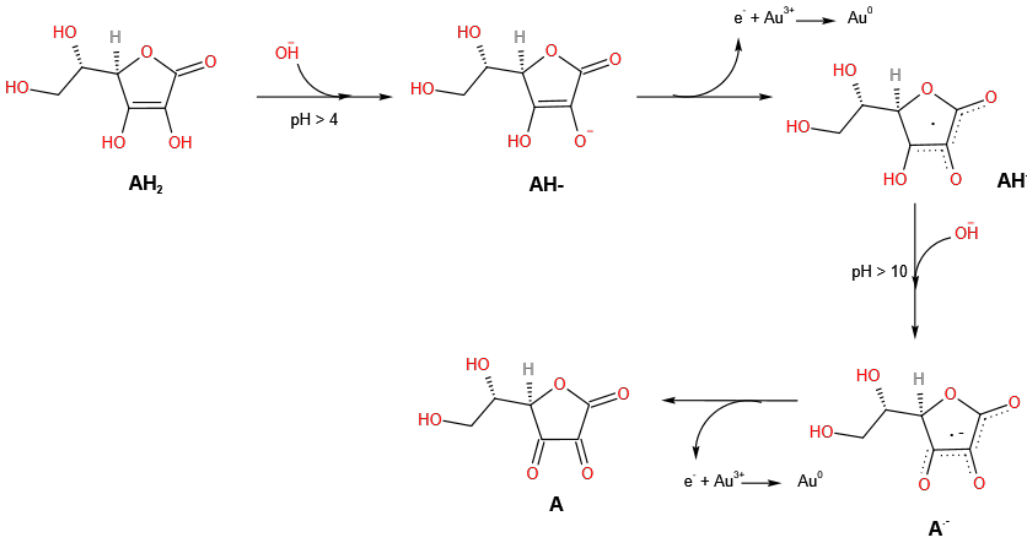

Figure 5. Description of the deprotonation process of ascorbic acid (AH_2) with increasing pH. The process also explains the capacity of AH_2 to reduce Au^{3+} to Au^0. At the same time, multiple molecules of AH_2 or deprotonated forms can coordinate to gold

Furthermore, as F. J. García De Abajo et al. [39] had suggested, the EELS probability results could provide direct information on the local photonic density of states (LDOS) [61] which plays a crucial role in plasmonic nanoparticles' optical properties [34,62].

5. Conclusions

Using soft acids to synthesize AuNPs combines functionality with suitable stability. Many experimental degrees of freedom and synthesis complexity require merging controlled experimental conditions and simplified yet relevant computational models. We used Ascorbic acid, AH_2, to synthesize non-spherical AuNPs in an aqueous solution with controlled pH via microwave-assisted synthesis and without any reducing agent. We show that, to some extent, the resulting AuNP shape depends on pH-microwave radiation. The combination of Transmission electron microscopy and UV-Vis spectroscopy of the adsorption of ascorbic acid on gold nanoparticle surface reveals a shape distribution and standard adsorption.

Furthermore, the plasmon modes are exposed by employing a qualitative simulation of electric field distribution and the electron energy loss probability map of the synthesized AuNPs. Ascorbic acid mainly binds to gold surfaces via its negative charge of the ascorbates group. Thus, pH 10 exhibits more robust binding to gold surfaces than lower pH values. The underlying mechanism in the Ascorbic acid-Au interaction deserves further examination, with reducing agents such as ascorbic acid and any other reducing-stabilizing agent whose structure is modified as pH changes.

Acknowledgments

R.BC. acknowledges the financial support from the National Research and Development Agency (ANID-Chile) National Ph.D. scholarship from ANID /National Doctorate (N° 2016–21160562). Additionally, R.BC thanks Dr. Charusheela Ramanan for her suggestions and discussions in this research and extended thanks to Max Planck Institute for Polymer Research (MPIP) for using the microwave reactor to carry out the synthesis, and thanked Katrin Kirchhoff from MPIP for helping us with the TEM and HR-TEM measurements. Likewise, R.BC. Thanks to Dr. Shirly Espinoza for providing the synthesis material. E.BM. acknowledges the financial support from PAIP-UNAM 5000-9192.

References

[1] U. Saxena and P. Goswami, "Electrical and optical properties of gold nanoparticles: Applications in gold nanoparticles-cholesterol oxidase integrated systems for cholesterol sensing," *J. Nanoparticle Res.*, vol. 14, no. 4, 2012,

[2] R. A. Dunlap, "Diamond," in *Novel Microstructures for Solids*, IOP Publishing, 2018.

[3] I. Hammami, N. M. Alabdallah, A. Al jomaa, and M. kamoun, "Gold nanoparticles: Synthesis properties and applications," *Journal of King Saud University - Science*, vol. 33, no. 7. 2021.

[4] M. Rafiee, S. Chandra, H. Ahmed, K. Barnham, and S. J. McCormack, "Small and large scale plasmonically enhanced luminescent solar concentrator for photovoltaic applications: modelling, optimisation and sensitivity analysis," *Opt. Express*, vol. 29, no. 10, 2021.

[5] H. B. Lee *et al.*, "Gap Plasmon of Virus-Templated Biohybrid Nanostructures Uplifting the Performance of Organic Optoelectronic Devices," *Adv. Opt. Mater.*, vol. 8, no. 11, 2020.

[6] C. Ma *et al.*, "Plasmonic-Enhanced Light Harvesting and Perovskite Solar Cell Performance Using Au Biometric Dimers with Broadband Structural Darkness," *Sol. RRL*, vol. 3, no. 8, 2019.

[7] H. Kang *et al.*, "Stabilization of Silver and Gold Nanoparticles: Preservation and Improvement of Plasmonic Functionalities," *Chem. Rev.*, vol. 119, no. 1, pp. 664-699, 2019.

[8] J. Dong, P. L. Carpinone, G. Pyrgiotakis, P. Demokritou, and B. M. Moudgil, "Synthesis of precision gold nanoparticles using Turkevich method," *KONA Powder Part. J.*, vol. 37, 2020.

[9] J. Turkevich, P. C. Stevenson, and J. Hillier, "A study of the nucleation and growth processes in the synthesis of colloidal gold," *Discussions of the Faraday Society*, vol. 11. 1951.

[10] C. J. Murphy *et al.*, "Anisotropic metal nanoparticles: Synthesis, assembly, and optical applications," *J. Phys. Chem. B*, vol. 109, no. 29, pp. 13857-13870, 2005.

[11] H. Yuan, Y. Liu, L. Tong, and Z. Wang, "Influence of Shape-Directing Agents on the Formation of Anisotropic Gold Nanoparticles," *Nano*, vol. 16, no. 9, 2021.

[12] B. Fleury, R. Cortes-Huerto, O. Taché, F. Testard, N. Menguy, and O. Spalla, "Gold Nanoparticle Internal Structure and Symmetry Probed by Unified Small-Angle X-ray Scattering and X-ray Diffraction Coupled with Molecular Dynamics Analysis," *Nano Lett.*, vol. 15, no. 9, 2015.

[13] E. Petryayeva and U. J. Krull, "Localized surface plasmon resonance: Nanostructures, bioassays and biosensing-A review," *Anal. Chim. Acta*, vol. 706, no. 1, pp. 8-24, 2011.

[14] Y. Hua, K. Chandra, D. H. M. Dam, G. P. Wiederrecht, and T. W. Odom, "Shape-Dependent Nonlinear Optical Properties of Anisotropic Gold Nanoparticles," *J. Phys. Chem. Lett.*, vol. 6, no. 24, pp. 4904-4908, 2015.

[15] N. N. Mallikarjuna and R. S. Varma, "Microwave-assisted shape-controlled bulk synthesis of noble nanocrystals and their catalytic properties," *Cryst. Growth Des.*, vol. 7, no. 4, pp. 686-690, 2007.

[16] K. W. Shah and L. Zheng, "Microwave-assisted synthesis of hexagonal gold nanoparticles reduced by organosilane (3-mercaptopropyl)trimethoxysilane," *Materials (Basel).*, vol. 12, no. 10, 2019.

[17] S. K. Seol, D. Kim, S. Jung, and Y. Hwu, "Microwave synthesis of gold nanoparticles: Effect of applied microwave power and solution pH," *Mater. Chem. Phys.*, vol. 131, no. 1-2, pp. 331-335, 2011.

[18] L. Ren, L. Meng, Q. Lu, Z. Fei, and P. J. Dyson, "Fabrication of gold nano- and microstructures in ionic liquids-A remarkable anion effect," *J. Colloid Interface Sci.*, vol. 323, no. 2, pp. 260-266, 2008.

[19] C. O. Kappe, "Controlled microwave heating in modern organic synthesis," *Angew. Chemie - Int. Ed.*, vol. 43, no. 46, pp. 6250-6284, 2004.

[20] B. L. Hayes, *Microwave Synthesis Chemistry at the Speed Light*. 2000.

[21] J. S. Schanche, "Microwave synthesis solutions from Personal Chemistry," *Mol. Divers.*, vol. 7, no. 2-4, pp. 293-300, 2003.

[22] H. Tyagi, A. Kushwaha, A. Kumar, and M. Aslam, "PH-dependent synthesis of stabilized gold nanoparticles using ascorbic acid," *Int. J. Nanosci.*, vol. 10, no. 4-5, pp. 857-860, 2011.

[23] S. Annur, S. J. Santosa, and N. H. Aprilita, "PH dependence of size control in gold nanoparticles synthesized at room temperature," *Orient. J. Chem.*, vol. 34, no. 5, pp. 2305-2312, 2018.

[24] M. Shopa, K. Kolwas, A. Derkachova, and G. Derkachov, "Dipole and quadrupole surface plasmon resonance contributions in formation of near-field images of a gold nanosphere," *Opto-Electronics Rev.*, vol. 18, no. 4, pp. 421-428, 2010.

[25] and G. C. S. K. Lance Kelly, Eduardo Coronado, Lin Lin Zhao, "The optical properties of metal nanoparticles: the influence of size, shape, and dielectric environment," *J. Phys. Chem. B*, vol. 107, no. 3, pp. 668-677, 2003.

[26] D. Radziuk and H. Moehwald, "Prospects for plasmonic hot spots in single molecule SERS towards the chemical imaging of live cells," *Phys. Chem. Chem. Phys.*, vol. 17, no. 33, pp. 21072-21093, 2015.

[27] R. Kumar *et al.*, "Plasmonic Au Nanoparticles Sensitized MoS for Bifunctional NO and Light Sensing," *IEEE Sens. J.*, vol. 21, no. 4, 2021.

[28] H. Kim *et al.*, "Ultrasensitive Near-Infrared Circularly Polarized Light Detection Using 3D Perovskite Embedded with Chiral Plasmonic Nanoparticles," *Adv. Sci.*, vol. 9, no. 5, 2022.

[29] B. Kumar, K. Smita, A. Debut, and L. Cumbal, "Andean Capuli Fruit Derived Anisotropic Gold Nanoparticles with Antioxidant and Photocatalytic Activity," *Bionanoscience*, vol. 11, no. 4, 2021,.

[30] Y. Guo and H. Thérien-Aubin, "Nanofibrous Photocatalytic Membranes Based on Tailored Anisotropic Gold/Ceria Nanoparticles," *ACS Appl. Mater. Interfaces*, vol. 13, no. 31, 2021.

[31] K. N. Clayton, J. W. Salameh, S. T. Wereley, and T. L. Kinzer-Ursem, "Physical characterization of nanoparticle size and surface modification using particle scattering diffusometry," Biomicrofluidics, vol. 10, no. 5, 2016, doi: 10.1063/1.4962992.

[32] M. Klinger and A. Jäger, "Crystallographic Tool Box (CrysTBox): automated tools for transmission electron microscopists and crystallographers ," *J. Appl. Crystallogr.*, vol. 48, no. 6, pp. 2012-2018, 2015.

[33] F. J. García de Abajo and A. Howie, "Retarded field calculation of electron energy loss in inhomogeneous dielectrics," *Phys. Rev. B - Condens. Matter Mater. Phys.*, vol. 65, no. 11, pp. 1154181-11541817, 2002.

[34] B. H. Lukas Novotny, *Principles of nano-optics*. Cambridge university press, 2012.

[35] U. Hohenester, "Simulating electron energy loss spectroscopy with the MNPBEM toolbox," *Comput. Phys. Commun.*, vol. 185, no. 3, pp. 1177-1187, 2014.

[36] U. Hohenester and A. Trügler, "MNPBEM - A Matlab toolbox for the simulation of plasmonic nanoparticles," *Comput. Phys. Commun.*, vol. 183, no. 2, pp. 370-381, 2012.

[37] A. Trügler, *Optical Properties of Metallic Nanoparticles : Basic Principles and Simulation*. Springer, 2016.

[38] A. Trügler, U. Hohenester, and F. J. García de Abajo, "Plasmonics simulations including nonlocal effects using a boundary element method approach," *Int. J. Mod. Phys. B*, vol. 31, no. 24, p. 1740007, 2017.

[39] F. J. García De Abajo and M. Kociak, "Probing the photonic local density of states with electron energy loss spectroscopy," *Phys. Rev. Lett.*, vol. 100, no. 10, pp. 1-4, 2008.

[40] B. Goris *et al.*, "Plasmon mapping in Au@Ag nanocube assemblies," *J. Phys. Chem. C*, vol. 118, no. 28, pp. 15356-15362, 2014.

[41] F. J. García de Abajo and A. Howie, "Relativistic electron energy loss and electron-induced photon emission in inhomogeneous dielectrics," *Phys. Rev. Lett.*, vol. 80, no. 23, pp. 5180-5183, 1998.

[42] P. B. Johnson and R. W. Christy, "Optical constants of the noble metals," *Phys. Rev. B*, vol. 6, no. 12, pp. 4370-4379, 1972.

[43] D. M. Pashkov *et al.*, "Quantitative Analysis of the UV-Vis Spectra for Gold Nanoparticles Powered by Supervised Machine Learning," *J. Phys. Chem. C*, vol. 125, no. 16, 2021.

[44] V. Myroshnychenko *et al.*, "Modelling the optical response of gold nanoparticles," *Chem. Soc. Rev.*, vol. 37, no. 9, pp. 1792-1805, 2008.

[45] E. G. Wrigglesworth and J. H. Johnston, "Mie theory and the dichroic effect for spherical gold nanoparticles: an experimental approach †," 2021.

[46] M. Finazzi and F. Ciccacci, "Plasmon-photon interaction in metal nanoparticles: Second-quantization perturbative approach," Phys. Rev. B - Condens. Matter Mater. Phys., vol. 86, no. 3, pp. 1–9, 2012, doi: 10.1103/PhysRevB.86.035428.

[47] Y. Yang *et al.*, "Upconversion emission enhancement of NaYF4:Yb,Er nanoparticles by coupling silver nanoparticle plasmons and photonic crystal effects," *J. Phys. Chem. C*, vol. 118, no. 31, 2014.

[48] M. Heo, H. Cho, J. W. Jung, J. R. Jeong, S. Park, and J. Y. Kim, "High-performance organic optoelectronic devices enhanced by surface plasmon resonance," *Adv. Mater.*, vol. 23, no. 47, 2011.

[49] H. Choi *et al.*, "Versatile surface plasmon resonance of carbon-dot-supported silver nanoparticles in polymer optoelectronic devices," *Nat. Photonics*, vol. 7, no. 9, 2013.

[50] A. Hörl, A. Trügler, and U. Hohenester, "Full Three-Dimensonal Reconstruction of the Dyadic Green Tensor from Electron Energy Loss Spectroscopy of Plasmonic Nanoparticles," *ACS Photonics*, vol. 2, no. 10, 2015.

[51] F. J. García De Abajo, "Optical excitations in electron microscopy," *Rev. Mod. Phys.*, vol. 82, no. 1, pp. 209-275, 2010.

[52] M. Kociak and O. Stéphan, "Mapping plasmons at the nanometer scale in an electron microscope," *Chemical Society Reviews*, vol. 43, no. 11. 2014.

[53] R. Baez-Cruz *et al.*, "Role of pH in the synthesis and growth of gold nanoparticles using L-asparagine: A combined experimental and simulation study," *J. Phys. Condens. Matter*, vol. 33, no. 25, 2021.

[54] M. Luty-Błocho, M. Wojnicki, and K. Fitzner, "Gold Nanoparticles Formation via Au(III) Complex Ions Reduction with L-Ascorbic Acid," *Int J Chem Kinet*, vol. 49, pp. 789–797, 2017.

[55] Z. Khan, T. Singh, J. I. Hussain, and A. A. Hashmi, "Au(III)-CTAB reduction by ascorbic acid: Preparation and characterization of gold nanoparticles," *Colloids Surfaces B Biointerfaces*, vol. 104, 2013.

[56] C. Gutiérrez-Wing, R. Esparza, C. Vargas-Hernández, M. E. Fernández García, and M. José-Yacamán, "Microwave-assisted synthesis of gold nanoparticles self-assembled into self-supported superstructures," *Nanoscale*, vol. 4, no. 7, pp. 2281-2287, 2012.

[57] C. Vargas-Hernandez, M. M. Mariscal, R. Esparza, and M. J. Yacaman, "A synthesis route of gold nanoparticles without using a reducing agent," *Appl. Phys. Lett.*, vol. 96, no. 21, pp. 1-4, 2010.

[58] L. Chen and G. Li, "Functions of 1-Dodecanethiol in the Synthesis and Post-Treatment of Copper Sulfide Nanoparticles Relevant to Their Photocatalytic Applications," *ACS Appl. Nano Mater.*, vol. 1, no. 9, 2018.

[59] M. B. Mohamed, K. M. Abouzeid, V. Abdelsayed, A. A. Aljarash, and M. S. El-Shall, "Growth mechanism of anisotropic gold nanocrystals via microwave synthesis: Formation of dioleamide by gold nanocatalysis," *ACS Nano*, vol. 4, no. 5, pp. 2766-2772, 2010.

[60] D. Njus, P. M. Kelley, Y. J. Tu, and H. B. Schlegel, "Ascorbic acid: The chemistry underlying its antioxidant properties," *Free Radical Biology and Medicine*, vol. 159. 2020.

[61] U. Hohenester, H. Ditlbacher, and J. R. Krenn, "Electron-energy-loss spectra of plasmonic nanoparticles," *Phys. Rev. Lett.*, vol. 103, no. 10, pp. 1-4, 2009.

[62] Stefan A. Maier, *Plasmonics: Fundamentals and Applications*. Springer Science & Business Media, 2007.

Supplementary Information

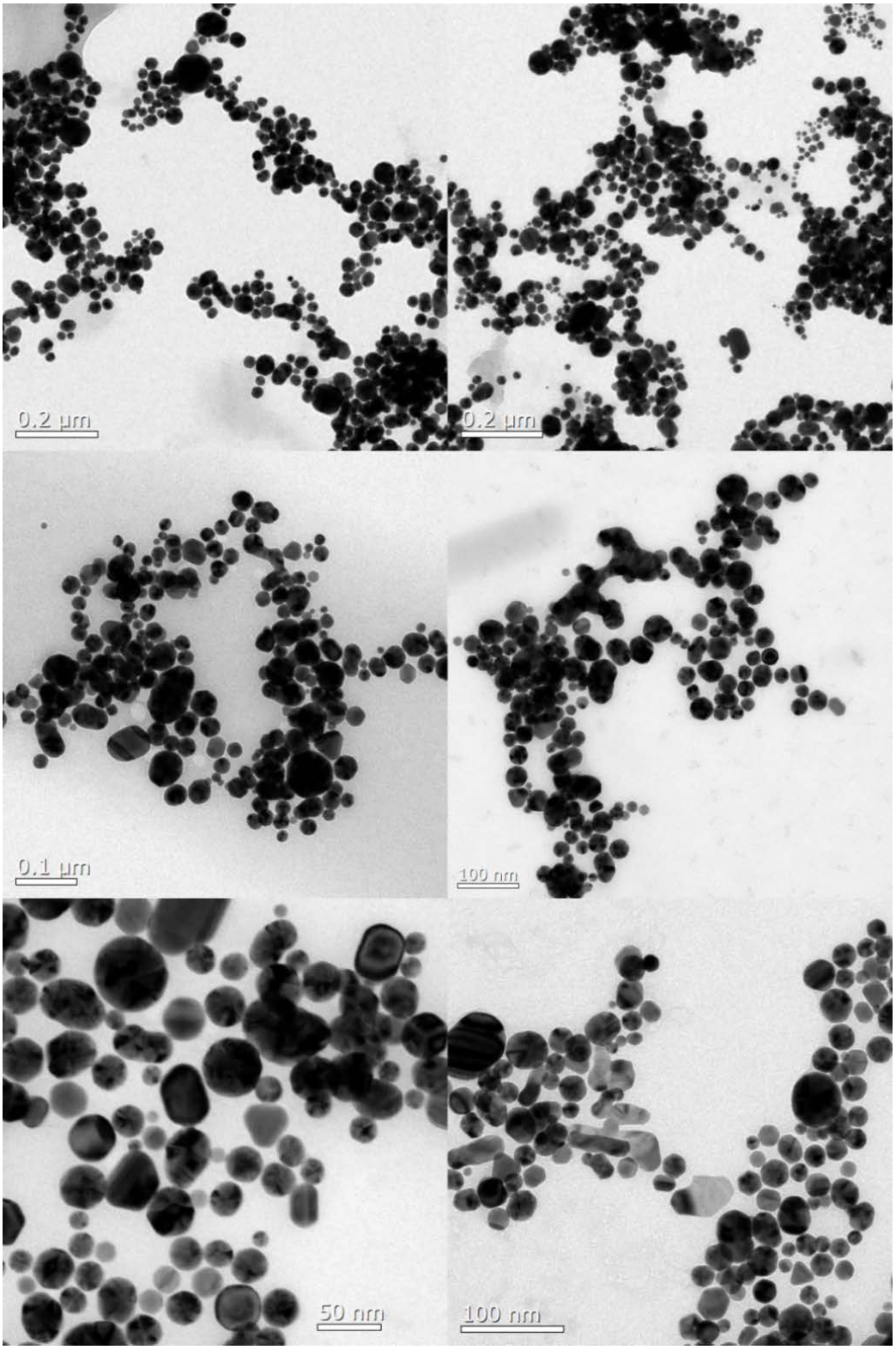

Figure S1. Gallery of a portion of TEM micrographs used to calculate the particle size distribution pH 10

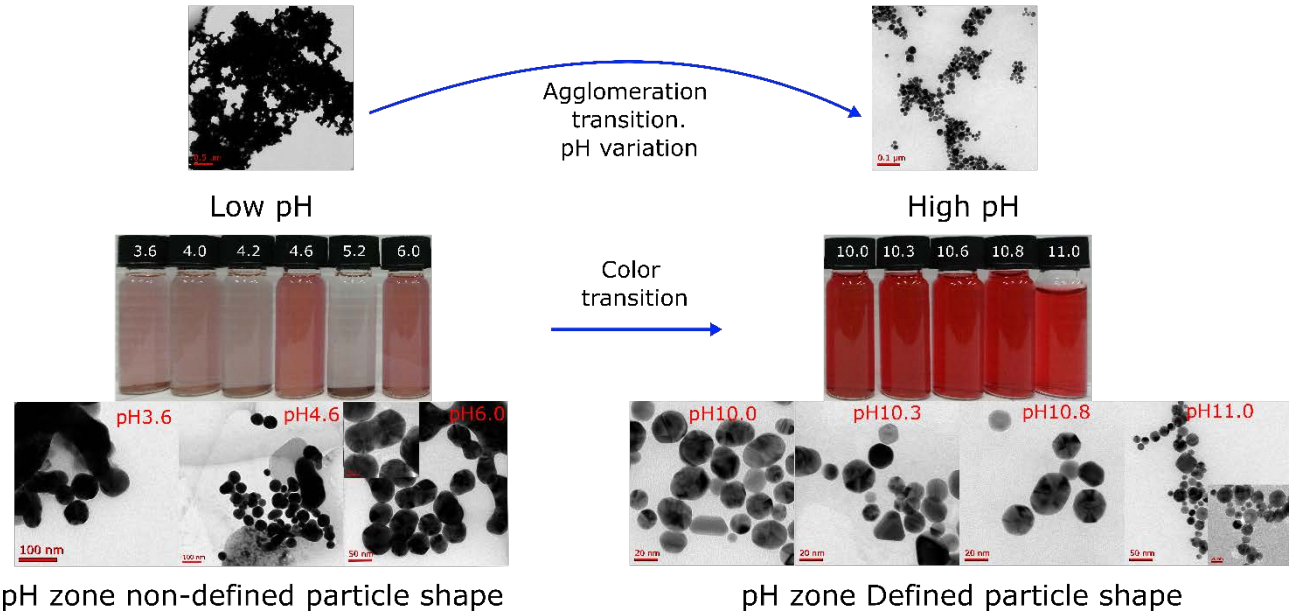

Figure S2. Comparison of sizes, shape, and color transition according to pH variation on gold nanoparticles synthesized